Spatial Sensing in Fibroblasts Mediated by 3′ Phosphoinositides✪

Jason M. Haugh,* Franca Codazzi,*‡ Mary Teruel,* and Tobias Meyer*

*Department of Cell Biology, Duke University Medical Center, Durham, North Carolina 27710;
and ‡Neuroscience Department, Dibit, San Raffaele Scientific Institute, Milan, Italy 20132

Abstract. The directed movement of fibroblasts towards locally released platelet-derived growth factor (PDGF) is a critical event in wound healing. Although recent studies have implicated polarized activation of phosphoinositide (PI) 3-kinase in G protein-mediated chemotaxis, the role of 3′ PI lipids in tyrosine kinase-triggered chemotaxis is not well understood. Using evanescent wave microscopy and green fluorescent protein–tagged Akt pleckstrin homology domain (GFP–AktPH) as a molecular sensor, we show that application of a shallow PDGF gradient triggers a markedly steeper gradient in 3′ PI lipids in the adhesion zone of fibroblasts. Polar GFP–AktPH gradients, as well as a new type of radial gradient, were measured from front to rear and from the periphery to the center of the ad-

hesion zone, respectively. A strong spatial correlation between polarized 3′ PI production and rapid membrane spreading implicates 3′ PI lipids as a direct mediator of polarized migration. Analysis of the temporal changes of 3′ PI gradients in the adhesion zone revealed a fast diffusion coefficient (0.5 $\mu m^2/s$) and short lifetime of 3′ PIs of <1 min. Together, this study suggests that the tyrosine kinase-coupled directional movement of fibroblasts and their radial membrane activity are controlled by local generation and rapid degradation of 3′ PI second messengers.

Key words: chemotaxis • signal transduction • phosphatidylinositol 3-kinase • receptor protein-tyrosine kinases • platelet-derived growth factor

Introduction

Wound repair and closure are achieved through the concerted efforts of multiple cell types (Martin, 1997). Important events in the healing process are the local secretion of platelet-derived growth factor (PDGF)[1] and the PDGF-mediated migration of fibroblasts into the wounded area (Seppa et al., 1982; Pierce et al., 1989; Deuel et al., 1991; Heldin and Westermark, 1999). This chemotactic response requires that fibroblasts can differentiate PDGF-mediated signaling at the front and rear. Spatial asymmetry in signaling (reviewed in Parent and Devreotes, 1999; Firtel and Chung, 2000) drives the polarized actin modifications required for lamellipodium extension and motility (Zigmond, 1996). Studies using green fluorescent protein (GFP) fusion

constructs in *Dictyostelium* and neutrophils have shown that 3′ phosphoinositides (PIs) generated upon activation of the G protein-coupled receptors are polarized towards the chemoattractant source (Parent et al., 1998; Meili et al., 1999; Servant et al., 2000). Furthermore, neutrophils that lack the γ isoform of PI 3-kinase exhibit a markedly suppressed chemotactic response for the tested G protein-coupled receptors (Hirsch et al., 2000; Li et al., 2000; Sasaki et al., 2000). This suggests that spatial regulation of PI 3-kinase activity plays an important role in controlling cell polarity during G protein-mediated chemotaxis.

It is therefore conceivable that the polarity of fibroblasts during PDGF-mediated chemotaxis is also controlled by polarized 3′ PIs, even though the PDGF signaling response is mediated by a tyrosine kinase and not a G protein-coupled signaling pathway and involves the activation of different PI 3-kinase isoforms (Claesson-Welsh, 1994; Vanhaesebroeck and Waterfield, 1999). Nevertheless, a role for PI 3-kinase in PDGF-initiated chemotaxis is supported by pharmacological studies demonstrating that PI 3-kinase activity is needed for migration towards PDGF (Kundra et al., 1994; Wennström et al., 1994).

The use of GFP fusion constructs has allowed both receptor- and lipid-mediated membrane translocation events in living cells to be observed in real time (Oancea and Meyer, 1998; Whitaker, 2000). While confocal micros-

copy has been the predominant imaging method used in these studies, its limited spatial-resolution of ∼500 nm reduces the precision of intracellular translocation measurements. As an alternative method, we built a microscope for evanescent wave excitation (Axelrod, 1981), in which a ∼70-nm layer adjacent to the glass-buffer interface is selectively illuminated. This allowed us to monitor 3′ PI production by measuring the translocation of the GFP-conjugated pleckstrin homology (PH) domain of Akt (GFP–AktPH) (Kontos et al., 1998; Watton and Downward, 1999; Meili et al., 1999; Servant et al., 2000) to the surface membrane with a much higher precision. We show that GFP–AktPH translocation in NIH 3T3 fibroblasts is spatially polarized in both the basal state and during exposure to a PDGF gradient, correlating with the direction of random migration and the induction of membrane spreading, respectively. Translocation in response to a uniform concentration of PDGF did not exhibit front-rear asymmetry in general, but rather displayed a radial pattern increasing in intensity from the center to the periphery of the contact area. The evolution of the radial profile was consistent with a rapid diffusion of 3′ PI lipids, and the radial gradients were exploited to determine the 3′ PI diffusion coefficient and turnover rate. Together, our results suggest that a local generation of 3′ PI lipids and their rapid degradation are key processes for spatial sensing in fibroblasts, governing directional migration through polar 3′ PI gradients and regulating cell shape by inducing selective membrane activity at the periphery of the adhesion area.

Materials and Methods

Reagents

Recombinant PDGF-BB was obtained from Peprotech, LY294002 and wortmannin were from Calbiochem, and cell culture reagents were from Life Technologies. Except where noted, all other chemical reagents were from Sigma-Aldrich.

cDNA Constructs and Transfection

Fusions of the Akt PH domain and Ha-Ras to the COOH terminus of enhanced GFP were made by cloning into the pEGFP-C1 vector (Clontech). A single base mutation in the Ha-Ras sequence was made by PCR, yielding the G12V insert. This was swapped for the wild-type sequence in Ha-Ras pEGFP-C1, and the resulting vector was made nonfluorescent by cutting out the EGFP sequence (Age I/BspEI) and ligating the (complementary) sticky ends. A nonfluorescent control vector was created in parallel, starting from pEGFP-C1 (pΔC1). The membrane-targeted enhanced GFP construct, with the modification sequence from Lyn (Teruel et al., 1999), was cloned into pcDNA3 (Invitrogen). NIH 3T3 fibroblasts were seeded onto 25-mm square glass coverslips, precoated with poly-D-lysine, for 24 h in growth medium. The cells were transiently transfected using lipofectamine Plus and OptiMEM I as the medium (Life Technologies); transfection and viability of fibroblasts were optimal after only 30–60-min incubation. After recovering in growth medium overnight, transfected cells were incubated in serum-free medium for 4 h before imaging. Additionally, cells were preincubated in the experimental buffer (20 mM Hepes pH 7.4, 125 mM NaCl, 5 mM KCl, 1.5 mM MgCl$_2$, 1.5 mM CaCl$_2$, 10 mM glucose, and 2 mg/mL BSA) for 15 min at the appropriate temperature.

Evanescent Wave Excitation and Fluorescence Microscopy

The setup was built around a Zeiss Axioskop 2 upright microscope with focusable water immersion objectives. A teflon ring is secured to the coverslip with grease to create an accessible buffer chamber. The sample is mounted on a self-built platform, with the coverslip optically coupled to a dove prism (Edmund Scientific) with immersion oil. The stage, but not the prism or microscope, can be moved in the x-y directions to view different

regions of the coverslip. The 488-nm excitation beam (10–40 mW, Coherent) is stabilized by a power controller (Cambridge Research & Instrumentation) and scrambled using a rotating diffuser (Physical Optical Corp.). The homogenized beam is refocused onto the prism at an angle yielding total internal reflection (>61° for a glass–water interface at 25°C). Alternatively, the beam can be directed to the back of the microscope, and down to the sample via a dichroic mirror (Chroma Inc.) for epifluorescence. In both cases, a 500–530-nm band pass filter (Chroma Inc.) was employed for emission. Images were recorded as a time series, using a cooled CCD video camera (Micromax 5 MHz, Princeton Instruments) and Universal Imaging software. The exposure time (typically 100–1,000 ms) was chosen based on an initial image so that no pixels in the region of interest would be saturated during the time course. The objective was cleaned twice each with methanol and deionized water between experiments. Stable temperature control was achieved using a plexiglass chamber to house the stage of the microscope, with minimal water evaporation (∼10%/h based on osmolarity) at 37°C.

Confocal Microscopy

A Zeiss 410 inverted laser scanning microscope (488-nm excitation, 500–530-nm emission) was used. Four 1-s scans were line-averaged.

Induction of PDGF Gradients

The concentration (C) of a solute, at a distance (r) from an injection point in an unstirred, semiinfinite medium, as a function of time (t), is given by,

$$C(r,t) = \frac{Me^{-r^2/(4Dt)}}{8(\pi Dt)^{3/2}}$$

where M is the absolute amount added, and D is the diffusion coefficient. Values for M and the approximate distance (r) were chosen so that the concentration of PDGF would approach its K_D in a reasonable time, with a significant gradient dC/dr. For example, for a solute with D = 100 μm^2/s, a bolus M = 1.5 pmol, injected 1 mm away will achieve C ∼0.01 nM at 3 min and C ∼1 nM at 5 min. Over this two log change in concentration spanning the observed K_D for PDGF, the relative gradient changes only modestly (2.8%/μm at 3 min and 1.7%/μm at 5 min). If the bolus is injected close to the coverslip in the z-direction (or if the velocity of the injection, neglected in the calculation above, brings it close to the coverslip), then the profile would spread as if in two dimensions relative to the cells; this modification does not dramatically affect the estimate of the relative gradient.

Mathematical Model of Membrane Second Messenger Dynamics

Formulation of the model equations is described in supplementary material. In the absence of probe prelocalization, there are six adjustable parameters: an observed consumption rate constant k_c; the dimensionless Dämkohler number Da = $k_c R^2/D$, where R is the effective radius of the contact area and D is the diffusion coefficient of the lipid; a dimensionless dissociation constant (κ) that compares the affinity of the fluorescent probe to the lipid generation rate at the top of the cell; a parameter (γ) that compares the generation rate at the top of the cell to the expression level of the fluorescent probe; the ratio of the generation rate in the contact area (bottom) to that of the top of the cell V_b/V_t; and a sensitivity coefficient (σ) describing the increase in intensity when a probe molecule is membrane-bound in the contact area versus freely diffusing in the cytosol. Fluorescence profiles were computed on a spreadsheet as a function of radial distance and time.

For the case of negligible production in the contact area ($V_b/V_t = 0$), Da was estimated to give the correct min/max ratio at steady state. The mean fold-increase in fluorescence at steady state is then determined by the sensitivity σ and the fraction of probe bound (calculated from κ and γ). These values were optimized such that the initial decrease in fluorescence at the center was also predicted properly. The values of κ and γ were then fine-tuned to capture the evolution of the profile shape over time, and finally k_c was specified to scale the profiles to real time. Thus, the parameters were not simultaneously fit to the data, but rather they were estimated successively to capture different aspects of the profiles.

Online Supplemental Material

The model equations used to simulate the GFP–AktPH distribution in Fig. 6 are included as an online appendix at http://www.jcb.org/cgi/content/full/151/6/1269/DC1.

Results

Evanescent Wave-imaging of GFP Constructs in the Membrane Adhesion Zone of Fibroblasts

A new design for an evanescent wave microscope was implemented to excite and monitor fluorescent molecules near the glass–water interface of an accessible cell chamber (Fig. 1 A and Materials and Methods). This imaging system included the capability to use low as well as high magnification objectives and to remotely scan the sample using micromotors. Evanescent wave microscopy, also known as total internal reflection fluorescence microscopy, has been used previously to study cell adhesion, binding to surfaces, and membrane trafficking (Axelrod, 1981; Thompson and Lagerholm, 1997; Burmeister et al., 1998; Schmoranzer et al., 2000; Toomre et al., 2000). As a novel application, we reasoned that such a microscope could be used to monitor translocation of GFP-tagged signaling proteins to or from the plasma membrane within the contact area of living, adherent cells. Our experimental setup also allowed for parallel epifluorescence excitation. Fig. 1 B shows unstimulated, GFP-transfected NIH 3T3 fibroblasts excited sequentially by epifluorescence and evanescent wave illumination. With the latter, only the adherent "footprint" of a cell is visualized. The high spatial resolution in the z direction results from a very short penetration depth of the excitation field (nominally ~70 nm). Since the illuminated sample is then effectively two-dimensional, the resolution in the x-y direction also improves and is set by the diffraction limit of light.

Compared with confocal microscopy, the selective excitation and higher spatial resolution of evanescent wave microscopy make it better suited for measuring plasma membrane recruitment of signaling proteins. The sensitivity of the technique was assessed by comparing the relative exci-
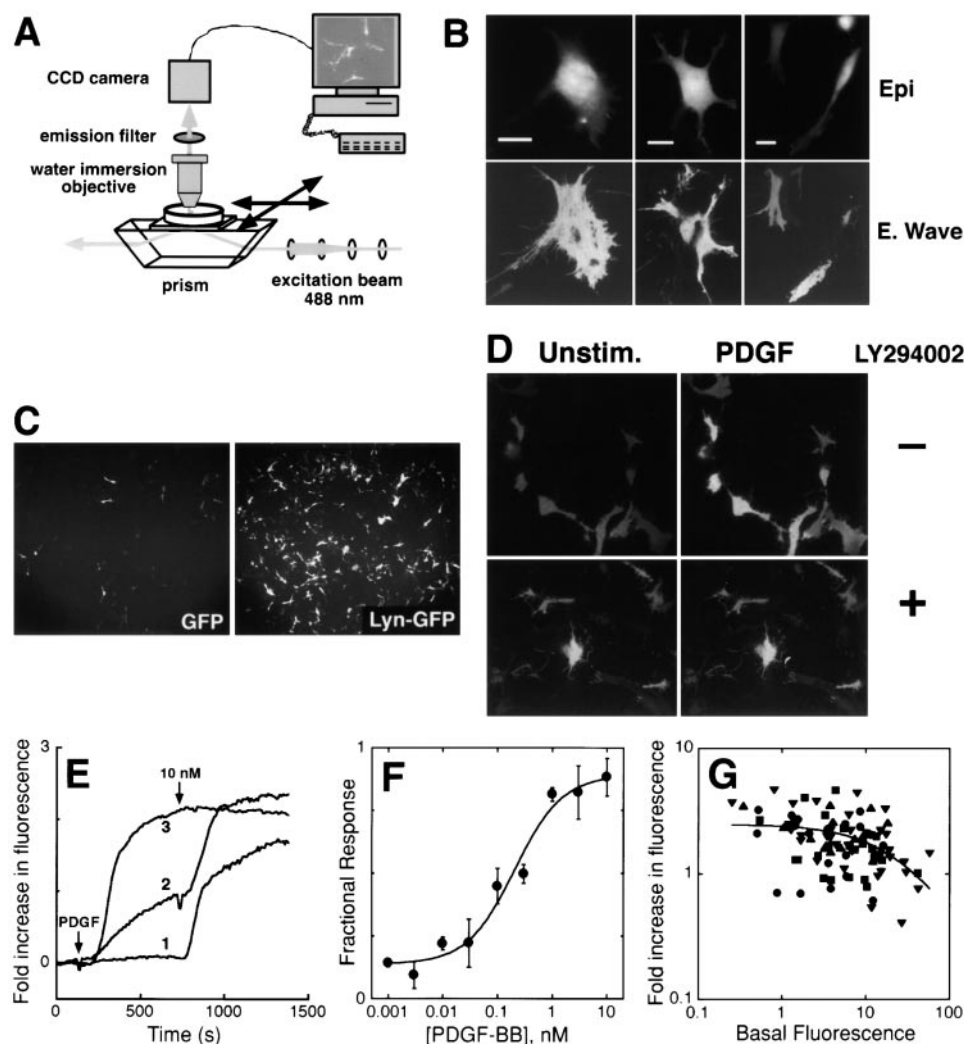

Figure 1. Evanescent wave imaging of PDGF-induced GFP–AktPH plasma membrane translocation in living fibroblasts. (A) Schematic view of the modified evanescent wave microscope design (see Materials and Methods for details). In short, the microscope uses water immersion objectives to image adherent cells in an open chamber, leaving the cells accessible for live cell experimentation. The 488-nm excitation laser beam is coupled through a prism below the coverslip and utilizes an oil drop between the coverslip and prism for light coupling, enabling total internal reflection from the glass–water interface. The coverslip is fixed on two sides to a motor controlled stage so that the cells can be moved in the x and y directions. (B) Comparison between evanescent wave and epifluorescence illumination. The same GFP-expressing NIH 3T3 fibroblasts were imaged using epifluorescence (top) and evanescent wave excitation (bottom). Bars, 20 μm. (C) Comparison of evanescent wave excited fluorescence intensities between soluble and plasma membrane-localized GFP. Low magnification images are shown of fibroblasts expressing GFP (left) or membrane-targeted GFP (Lyn-GFP, right). (D) Evanescent wave images of NIH 3T3 fibroblasts expressing a GFP fusion of the Akt PH domain (GFP–AktPH) captured before (left) and 5 min after (right) addition of PDGF-BB. Translocation was blocked by 100 μM LY294002, a specific inhibitor of PI 3-kinases (bottom). (E) Representative translocation responses of individual GFP–AktPH-transfected fibroblasts in response to 1–30 pM, 100–300 pM, or 1–10 nM PDGF-BB at room temperature. A second dose adjusted the PDGF concentration to 10 nM. (F) Dose response of PDGF-induced GFP–AktPH translocation, normalized by the response to a second, maximal dose. The responses of cells in the same field were compiled, and the data points are averaged over experiments on three separate days ($\pm$ SEM, n = 3). (G) The fold increase in fluorescence intensity stimulated by a maximal PDGF dose is plotted for individual cells, as a function of the prestimulus fluorescence intensity normalized by the beam power*exposure time (mJ). The symbols signify experiments performed on different days.
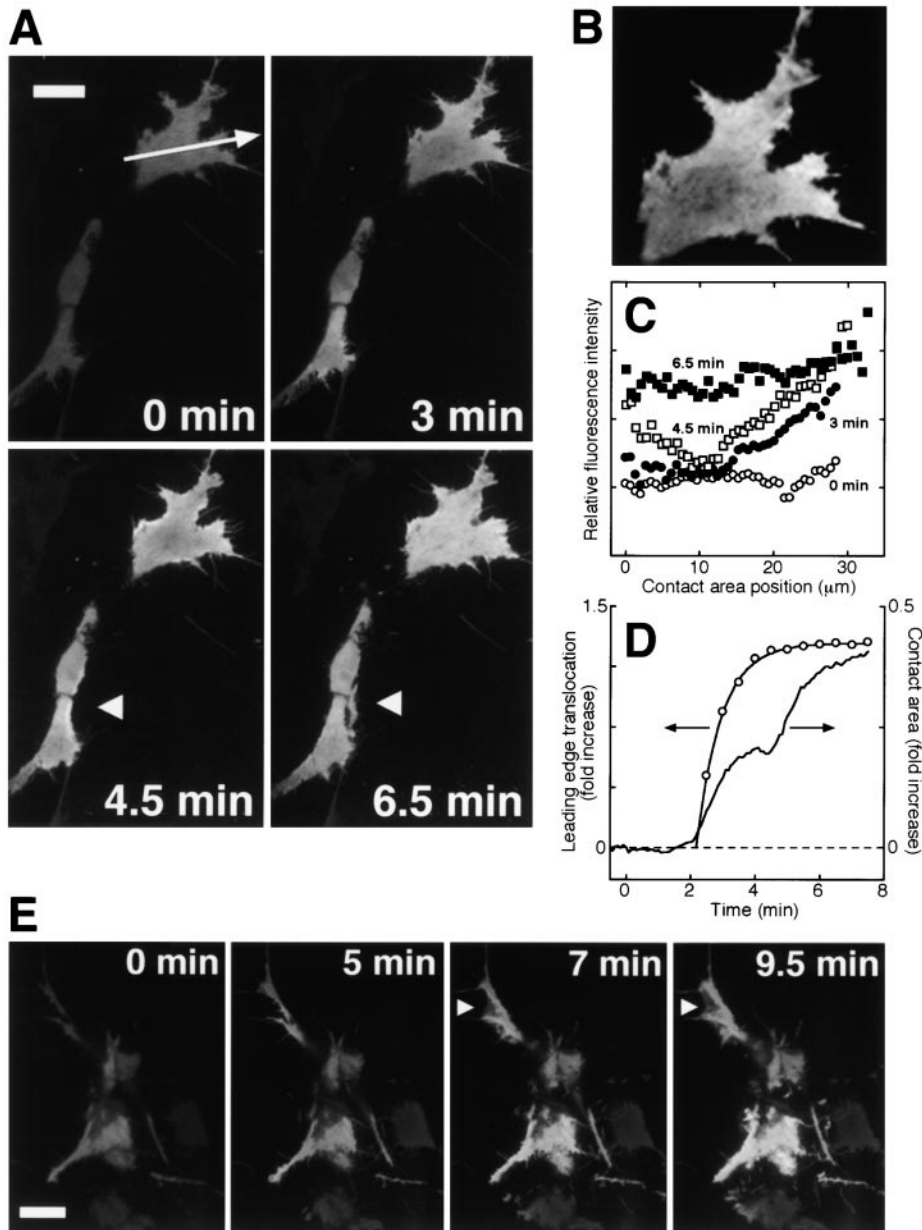
Figure 2. Induction of 3′ PI lipid gradients and polarized membrane spreading in response to PDGF gradients. (A) Time series of evanescent wave images showing GFP–AktPH-transfected NIH 3T3 fibroblasts responding to a transient PDGF-BB gradient at 37°C (PDGF diffusing in from the right). The arrows in the bottom panels mark a membrane extension event on the side of a cell that was initially oriented towards the bottom of the field. (B) Magnification of the cell in the upper right of A, 3-min time point. (C) Surface-proximal fluorescence profiles for the cell in A and B at various time points after PDGF addition. The arrow in the first panel of A shows the position and direction of the line scan. (D) Comparison of the time course of GFP–AktPH translocation and membrane spreading. GFP–AktPH fluorescence increase at the leading edge was compared with the increase in total contact area spreading (for the top cell described in A–C). (E) Time series of localized translocation as in A, except PDGF is diffusing from the left. The arrows mark an apparent lamellipodial extension. A and E are representative of six separate experiments. Bars, 20 μm.

tation of a membrane-targeted GFP (using the palmitoylation–myristoylation sequence from Lyn) to that of soluble GFP (Fig. 1 C). Evanescent wave microscopy detects membrane localization simply as an elevated fluorescence intensity, allowing many cells to be observed at low magnification, as shown in Fig. 1 C. After normalization by the epifluorescence signal for each cell (data not shown), it was determined that excitation of the membrane-targeted GFP was ∼12-fold higher than for soluble GFP. The dynamic range of the assay for the relatively thin fibroblasts is therefore estimated to be over an order of magnitude.

GFP-labeled PH domains have been employed as quantitative molecular sensors to measure the local concentration of PI lipids in living cells over time (Stauffer et al., 1998). Several pleckstrin homology (PH) domains bind specifically to the 3′ PIs $PI(3,4,5)P_3$ and $PI(3,4)P_2$ (Lemmon et al., 1996; Czech, 2000), and the GFP-conjugated PH domain of Akt has been used effectively as a fluorescent biosensor for 3′ PI lipids (Kontos et al., 1998; Watton and Downward, 1999; Meili et al., 1999; Servant et al., 2000).

Fig. 1 D shows the increase in surface-proximal fluorescence intensity observed for NIH 3T3 fibroblasts, transfected with GFP–AktPH, after stimulation with PDGF at room temperature (∼25°C). Stimulated translocation of this probe was robust and easily measured by evanescent wave microscopy. The PI 3-kinase inhibitors LY294002 (100 μM, Fig. 1 D) or wortmannin (100 nM, not shown), but not vehicle alone, completely abolished GFP–AktPH translocation in our assay, suggesting that this probe binds specifically to 3′ PIs.

Evanescent Wave Microscopy Is Suitable for Monitoring Signal Transduction Events at Physiological Agonist Concentrations

Representative kinetic traces of PDGF-stimulated GFP–AktPH translocation are shown in Fig. 1 E, showing minimal, intermediate, and maximal translocation responses. In accord with previous studies, maximal translocation was long-lived on the time scale of minutes (Watton and
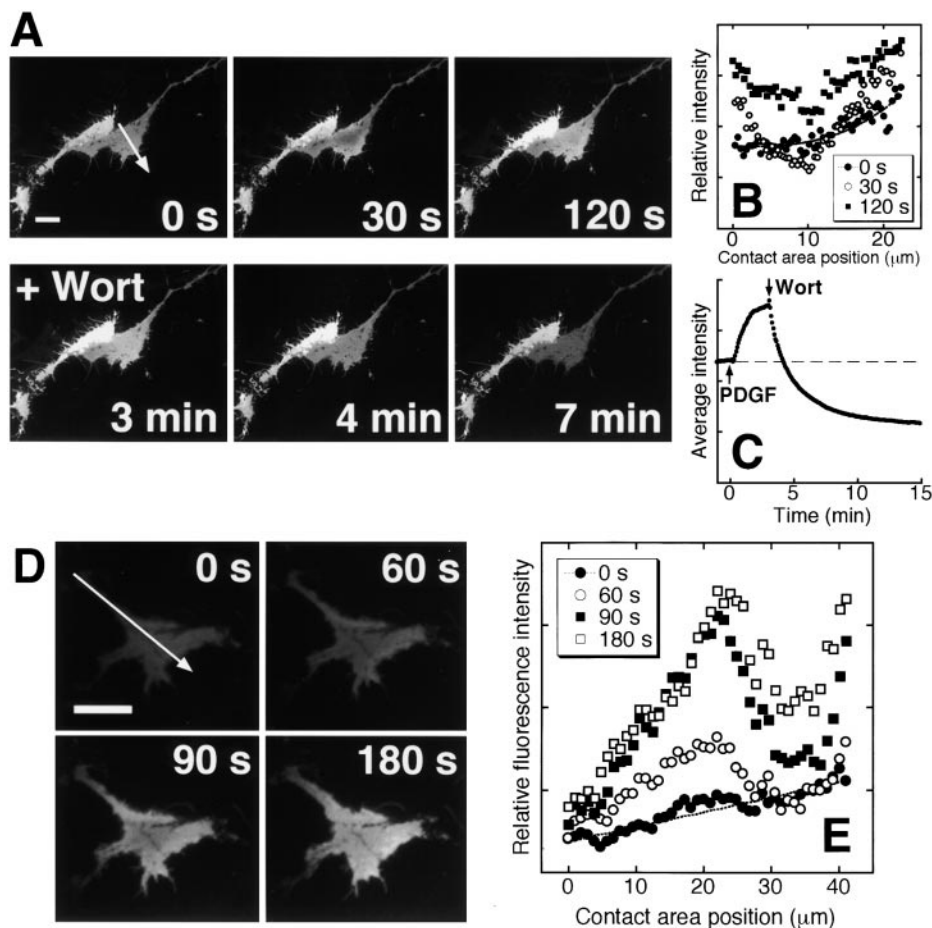
Figure 3. Basal gradients in 3′ PI lipids correlate with cell orientation. (A) Evanescent wave images of GFP–AktPH-transfected NIH 3T3 fibroblasts at 37°C, showing basal 3′ PI gradients and a more symmetrical response after uniform PDGF-BB stimulation (5 nM). PI 3-kinase activity was rapidly inhibited after 3 min by the addition of wortmannin (Wort). (B) Spatial fluorescence profiles for the cell on the right in A. (C) Time course, average fluorescence intensity in the contact area for the cell in A and B. (D) Evanescent wave images of a representative GFP–AktPH-transfected fibroblast at low cell density, stimulated with a uniform dose (5 nM) of PDGF-BB at 37°C. (E) Spatial fluorescence profiles for the cell in D. All arrows indicate the position and direction of the line scans used to generate spatial profiles. Bars, 20 μm.

Downward, 1999). The dose response curve indicates that half-maximal translocation is achieved at a PDGF concentration yielding roughly half-maximal receptor binding ($\sim$0.2 nM; Fig. 1 F). This is consistent with the absence of major bottlenecks between receptor binding and probe translocation, such as significant depletion of GFP–AktPH from the cytosol at submaximal PDGF doses. The slower translocation kinetics at intermediate doses (Fig. 1 E) is also consistent with receptor binding of PDGF being the rate-limiting step.

Although the affinities between PH domains and PI lipids measured in vitro are relatively low, it is still conceivable that most of the produced 3′ PI molecules are sequestered by the GFP–AktPH domains, thereby mediating a dominant-negative effect. If this were the case, the fold increase in surface-proximal fluorescence would be a decreasing function of the probe expression level. However, while the basal fluorescence varied over two decades of expression, the maximum fold increase in fluorescence intensity varied over a much smaller range, with no apparent reduction for all but the highest expressers (Fig. 1 G). This is consistent with most 3′ PIs remaining available for binding cellular targets except in cells that express the highest concentrations of GFP–AktPH domains. Thus, we do not attribute the observed plateau in GFP–AktPH translocation (Fig. 1 E) to interference with 5′ phosphatases and a possible suppression of the normally transient PI(3,4,5)P$_3$ response, but rather to the ability of the probe to bind the less transient PI(3,4)P$_2$ lipid at least equally well (Frech et al., 1997; Kavran et al., 1998; Gray et al., 1999).

Extracellular PDGF Gradients Trigger Markedly Steeper Intracellular Gradients in 3′ Phosphoinositide Lipids

The translocation of GFP–AktPH in response to a gradient of PDGF was assessed in a temperature-controlled chamber to maintain the microscope stage at 37°C. A gradient in PDGF concentration was generated by slowly injecting a small bolus of PDGF (1.5 pmol in 5 μL) $\sim$1 mm from the cells. With this approach, the average PDGF concentration seen by the cells increases over time, with half-maximal receptor binding occurring within minutes. The PDGF gradient, in relative terms, is estimated to be robust, maintained at 1–3% per micrometer before the saturation of PDGF receptors (Materials and Methods). Control experiments using fluorescent dextran were in agreement with these estimates (data not shown).

When PDGF was introduced by this method, GFP–AktPH translocation was consistently polarized towards the PDGF source. Strikingly, the region with the highest concentration of GFP–AktPH invariably exhibited membrane activity and the formation of lamellipodia (in six experiments, each observing two or more cells). Further, the bias in GFP–AktPH translocation and membrane extension did not depend on the orientation of the cells before stimulation with the PDGF gradient. In Fig. 2 A, PDGF was introduced from the right, and asymmetric translocation was apparent by 2–3 min. The pronounced left-right gradient in fluorescence intensity for the cell in the upper right is shown in more detail in Fig. 2 B, and fluorescence
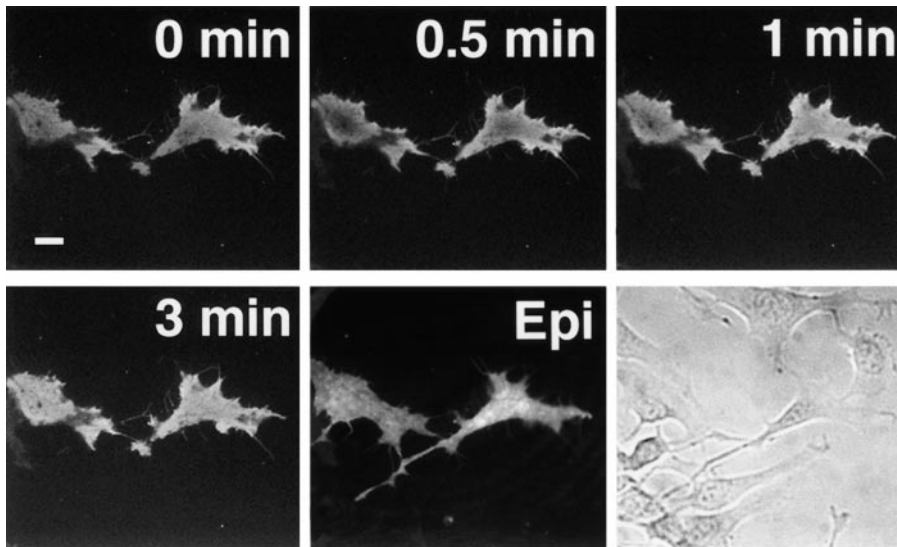
profiles for this cell are shown in Fig. 2 C. Coinciding with the onset of GFP–AktPH translocation, the same cell also began spreading rapidly towards the stimulus. An analysis of the time courses of local GFP–AktPH translocation versus total cell spreading is shown in Fig. 2 D. For later time points, the average PDGF level is sufficient to dimerize all receptors, and the translocation profile becomes more symmetrical (Fig. 2 C). The disparate kinetics of translocation on the right and left sides for this cell are temporally and spatially consistent with the two plateaus visible in the contact area spreading time course in Fig. 2 D.

Fig. 2 E shows a similar experiment in which the stimulus was directed from the left. In control experiments, pretreatment with LY294002 (100 μM) blocked both GFP–AktPH translocation as well as membrane spreading (data not shown). These results indicate that PI 3-kinase-dependent actin mobilization stimulated by PDGF is spatially focused by the localized generation of 3′ PI lipids.

Correlation of Cell Orientation and 3′ Phosphoinositide Gradients in Unstimulated Cells

An interesting feature observed for most cells was the presence of preexisting basal polarity in GFP–AktPH localization. Such basal 3′ PI gradients were observed in nearly confluent as well as in low density fibroblast cultures at 37°C, whereas basal gradients were far less prominent at room temperature. Fig. 3, A and B, show basal intensity gradients in a representative experiment using nearly confluent fibroblasts. Uniform PDGF stimulation rapidly equalized the gradients on both sides of the contact area, and subsequent addition of wortmannin caused a rapid decay in fluorescence below the prestimulus level (Fig. 3 C) and an ablation of the basal fluorescence gradient (data not shown).

Fibroblasts plated at lower density also exhibited 3′ PI gradients in the basal state, correlating with an apparently migratory morphology. A representative example of such a cell is shown in Fig. 3 D, for which a marked linear gradient in GFP–AktPH translocation was observed (Fig. 3 E). In response to uniform PDGF stimulation, two distinct spatial regimes became apparent. For the adhesion perimeter around the apparent cell body, PDGF caused the intensity to be equalized, leading to a U-shaped steady state

profile similar to Fig. 3 B. In contrast, a linear gradient was maintained in the tail. Following uniform PDGF stimulation, the slope of this tail gradient increased with time, with the fluorescence intensity at the very rear of the cell increasing only modestly compared with the cell body. These results are consistent with a spatial regulation of 3′ PI levels during cell migration.

3′ Phosphoinositide Gradients in Wounded Monolayers

Given that fibroblast migration is inhibited by contact with adjoining cells, and that 3′ PI generation appeared to be polarized away from neighboring cells (for example Fig. 3 A), we hypothesized that the basal PI 3-kinase activity and cell orientation are related phenomena. To test this hypothesis further, we biased cell orientation by wounding a monolayer of quiescent, GFP–AktPH-transfected fibroblasts (Fig. 4; representative experiment selected from five separate experiments conducted at 37°C). Cells at the interface were oriented towards the acellular area by 1–2 h, after which the basal and PDGF-stimulated fluorescence patterns were assessed. All of the cells observed exhibited an apparent prestimulus 3′ PI gradient directed away from adjacent cells, with markedly brighter fluorescence associated with lamellipodia and filopodia. As in Fig. 3, the uniform addition of PDGF equalized the circumference fluorescence profile (in 4 of 5 wounding experiments), and addition of wortmannin rapidly erased all fluorescence gradients.

Radial 3′ Phosphoinositide Lipid Gradients in the Cell–Surface Contact Area

The ability of 3′ PI lipids to locally enhance actin cytoskeletal activity suggests an important role in directed migration. However, this function of 3′ PIs may also regulate the size and shape of adhesive contact areas. Consistent with this hypothesis, cells with significant adhesion areas reproducibly showed radial 3′ PI gradients that increased from the center to the periphery of the contact area (for example, Fig. 3, A and D). These gradients were investigated quantitatively at room temperature (∼25°C), since the lower temperature significantly suppressed basal 3′ PI gradients as well as membrane activity and spreading in response to PDGF stimulation.
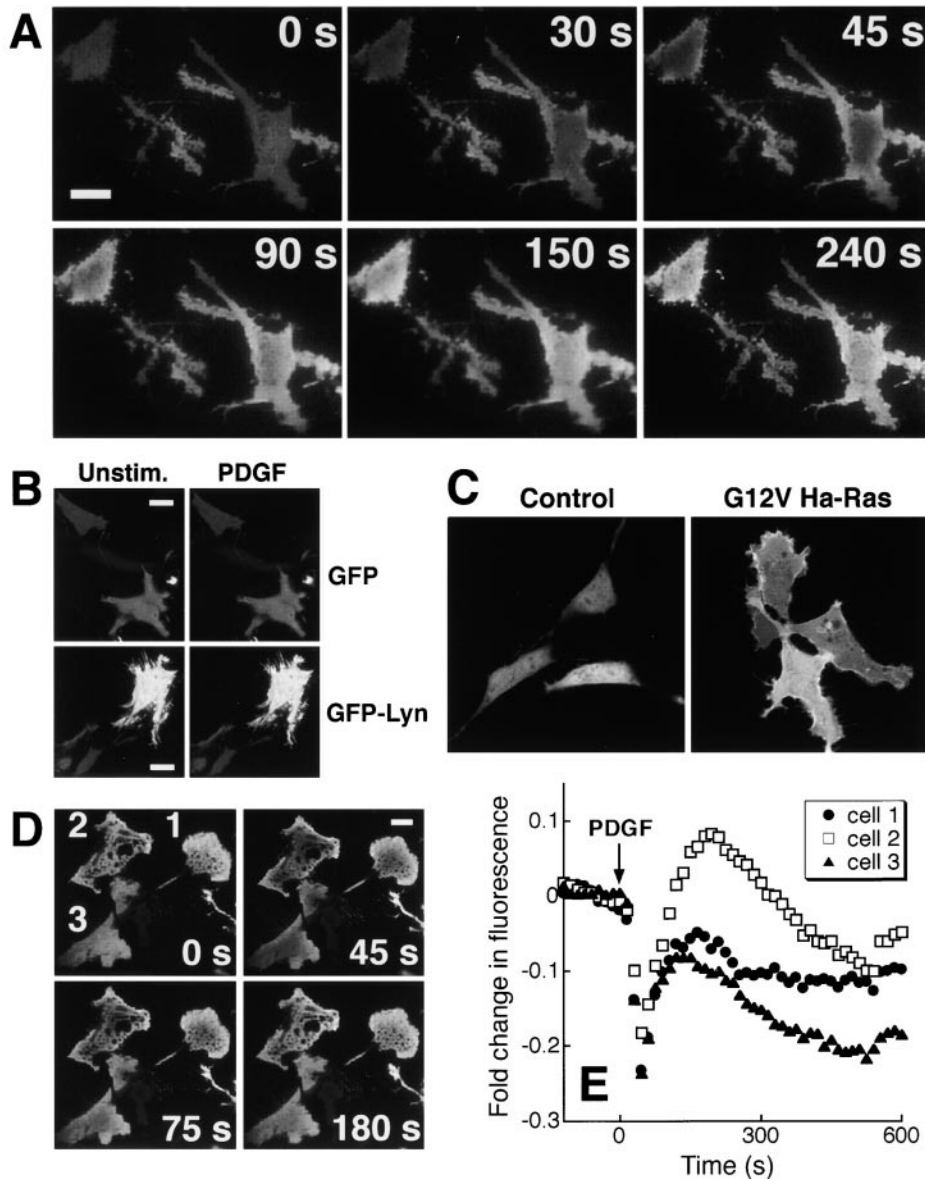
Figure 5. PDGF-stimulated radial 3′ PI gradients in the cell contact area. (A) Representative translocation response of GFP–AktPH-transfected NIH 3T3 fibroblasts to uniformly maximal PDGF-BB stimulation at room temperature, showing radial gradients in GFP–AktPH translocation with low intensities in the center and high intensities at the periphery. (B) Control experiments with soluble and membrane-targeted GFP show uniform fluorescence intensities that are not significantly changing with PDGF stimulation. Representative evanescent wave images of fibroblasts expressing GFP (top) or Lyn-GFP (bottom) were captured before (left) and 5 min after (right) addition of PDGF-BB. (C) Confocal fluorescence images of unstimulated NIH 3T3 fibroblasts cotransfected with GFP–AktPH and either a control vector (pΔC1) or G12V Ha-Ras. The coexpressed activator of PI-3 kinase induces a strong localization of GFP–AktPH in unstimulated cells. (D) Evanescent wave images showing fibroblasts, cotransfected with GFP–AktPH and G12V Ha-Ras, and responding to PDGF stimulation at 37°C show a marked initial decrease in fluorescence intensity. (E) Time course of the average fluorescence intensity for each of the cells in D. Bars, 20 μm.

Fig. 5 A shows the translocation responses of two representative cells to uniform PDGF stimulation. After a lag period, uniform PDGF stimulation triggered a uniform fluorescence intensity increase around the periphery of the contact area, followed by an increase in fluorescence in the center as well as the periphery. Importantly, control experiments showed that larger cells expressing soluble or membrane-targeted GFP did not exhibit radial gradients, allowing several possible artifacts to be ruled out. These include variations in the membrane–substratum separation distance, edge artifacts caused by the concentration of membrane at the periphery, and extensive photobleaching. PDGF elicited neither changes in the mean fluorescence intensity nor the formation of spatial gradients in these cells (Fig. 5 B and data not shown).

Surprisingly, the radial asymmetry was not caused by exclusion of PDGF from the contact zone. When fluorescent dextrans (up to 40 kD) were added in control experiments, the intensity underneath a cell was 50–70% of the fluorescence intensity elsewhere, and there was no significant lag in the intensity increase (data not shown). The slightly lower fluorescence intensity beneath the cells is an expected result from the presence of the cell within the evanescent wave-illuminated region. This indicates that the reduced concentration of 3′ PI lipids in the contact area was not caused by a lack of PDGF access, but suggests instead a segregation or feedback regulation of signaling components between the nonadherent and the adherent plasma membrane. Thus, we hypothesized that the radial pattern of 3′ PI lipids is produced by production of 3′ PI lipids in the nonadherent membrane, diffusion of 3′ PIs from the periphery into the contact area, and degradation of 3′ PI lipids within the contact area.

To further test this hypothesis, the translocation of GFP–AktPH was enhanced by coexpression with the GTPase-deficient (and therefore constitutively active with respect to signaling) G12V Ha-Ras variant. G12V Ras is expected to elicit PI 3-kinase activity independently of, and synergistically with, PDGF stimulation (Rodriguez-Viciana et al., 1994, 1996; Klinghoffer et al., 1996). Indeed, coexpression with G12V Ras is sufficient to prelocalize most of the GFP–AktPH to the membrane as observed using confocal
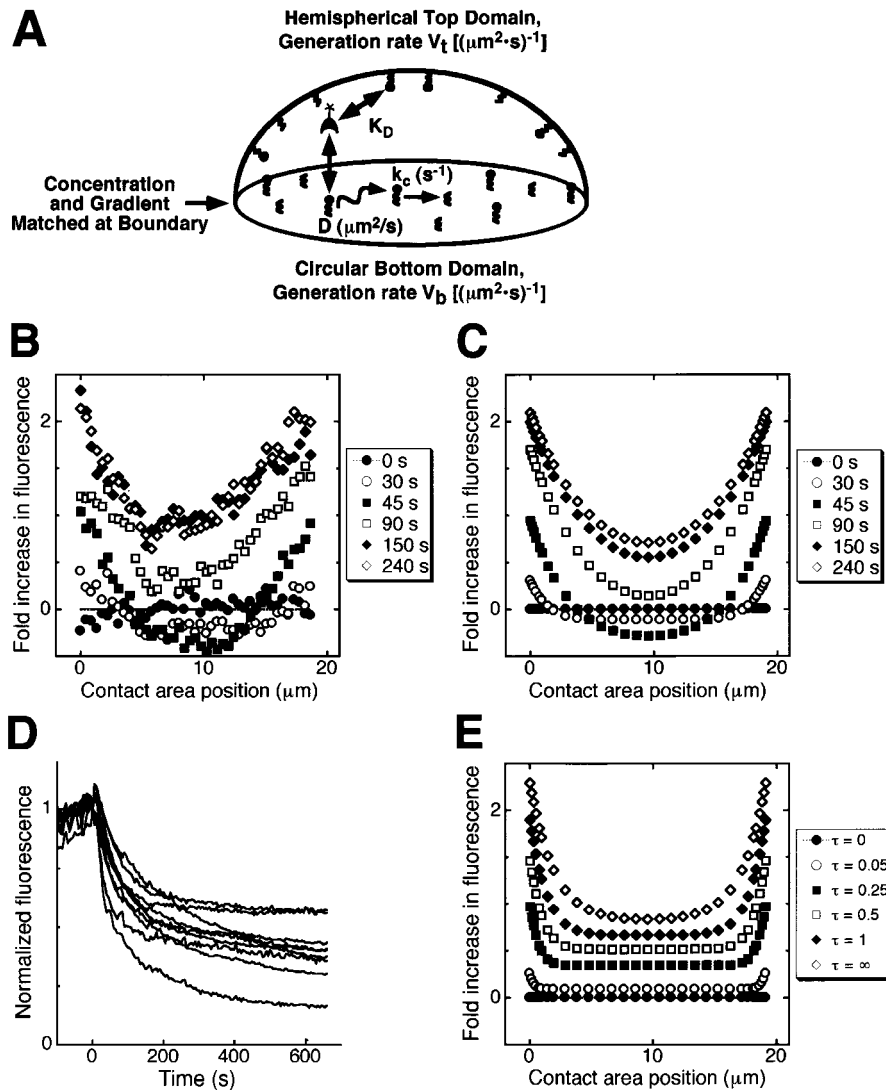
A

B **C**

D **E**

Figure 6. Model calculations enable a determination of the diffusion coefficient and lifetime of 3′ PI lipids. (A) Model schematic. The mathematical model accounts for lipid generation, characterized by a reaction velocity V, lipid diffusion, characterized by a diffusion coefficient D, and lipid consumption, characterized by the rate constant k_c. The expression level and equilibrium dissociation constant K_D of the fluorescent probe are also accounted for. (B) Experimental fluorescence profiles measured for the cell on the right in Fig. 5 A. (C) Theoretical fluorescence profiles, assuming that no 3′ PI lipids are generated in the contact area ($V_b/V_t = 0$). Other model parameters were optimized to match various aspects of the experimental profiles in B (Materials and Methods): D = 0.5 $\mu m^2/s$, k_c = 1 min^{-1} (Da = $k_c R^2/D = 3$), $\kappa = 1/3$, $\gamma = 3$, $\sigma = 14$. In accord with the early time points of the series in Fig. 5 A (not shown), a time lag of 25 s was built into the model. (D) Experimental determination of the degradation rate constant k_c by rapidly inhibiting PI 3-kinase activity. GFP–AktPH-expressing fibroblasts were maximally stimulated with PDGF-BB for 5 min, after which 250 μM LY294002 was added (time zero). (E) An alternative model assuming significant second messenger generation in the contact area yields poor agreement with experiment. Computed profiles are shown for different normalized times $\tau = k_c \ast t$, with the parameter values in C except Da = 30, $V_b/V_t = 0.35$.

microscopy (Fig. 5 C). Using evanescent wave excitation, the average surface-proximal fluorescence transiently decreased by ∼25% following a maximal dose of PDGF (Fig. 5 D and E). The drop in fluorescence suggests that GFP–AktPH is initially lost from the contact area due to a competition with 3′ PI lipids produced outside the contact region, supporting the hypothesis of much higher 3′ PI production in the nonadherent region.

Local Generation, Diffusion, and Degradation of 3′ Phosphoinositides

To determine how spatial gradients in 3′ PI lipids can be generated, the diffusion coefficient and degradation times of 3′ PI lipids were determined by comparing the radial patterns in GFP–AktPH translocation elicited by PDGF with a mathematical model of lipid second messenger dynamics (see http://www.jcb.org/cgi/content/full/151/6/1269/DC1). A key feature of the model is that the nonadherent portion of the plasma membrane, modeled as a hemisphere, and the circular contact area can have different second messenger production rates. The lipid diffuses laterally with observed mobility coefficient D, and it is con-

sumed by first order reaction(s) with observed rate constant k_c in both domains (Fig. 6 A). As a representative experiment, the spatial profiles across the width of the cell on the right in Fig. 5 A are plotted in Fig. 6 B (the cell on the left exhibited similar behavior). The profile before stimulation was flat, and, during the first stages of the translocation response, the intensity in the center of the contact area actually decreased. A smooth, U-shaped profile was established within 45 s of stimulation, attaining a steady state by 2–3 min.

Fig. 6 C shows model calculations assuming negligible second messenger production in the contact area. The other parameters were adjusted to yield agreement with Fig. 6 B (see Materials and Methods), capturing all quantitative aspects of the experimental profiles. For example, the fluorescence decrease in the center of the profile is attributed to the depletion of GFP–AktPH from the cytosol, with diffusion being too slow to compensate for early time points. Of particular interest are the estimated values of the 3′ PI diffusion coefficient D (∼0.5 $\mu m^2/s$) and specific turnover rate k_c (∼1 min^{-1}). The estimated diffusion coefficient is in approximate agreement with mobility studies of membrane lipid probes and Ras, which is lipid-
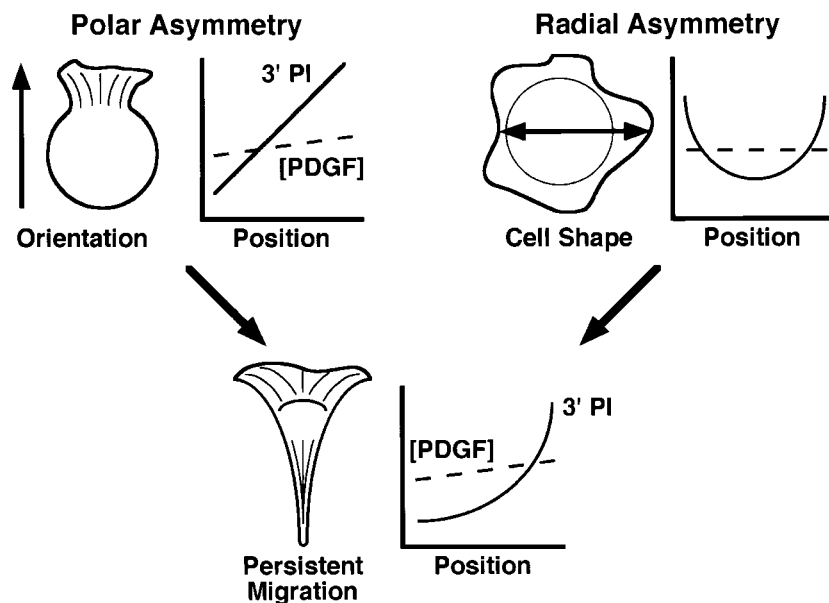
Figure 7. Proposed dual roles of 3′ PIs in fibroblast motility. The model assumes that multiple spatial cues, including gradients of PDGF and immobilized ligands that mediate adhesion, are integrated over space and time at the level of 3′ PI distribution in the membrane to generate polarized cell migration. Polar (front-back) asymmetry in 3′ PI generation leads to a bias in the orientation of membrane extension. At the same time, cell adhesion regulates signaling from PDGF receptors, leading to radial asymmetry in 3′ PI concentration within the contact area. The important parameter is the ratio of 3′ PI diffusion to degradation, which determines the range of the second messenger. This suggests a shaping mechanism in which 3′ PI level contributes to cell spreading, but the increase in adhesion limits signal propagation. These two modes of spatial asymmetry would cooperate to focus 3′ PI distribution at the leading edge for optimal migration.

anchored (Schlessinger et al., 1977; Niv et al., 1999). To estimate the degradation rate constant independently, GFP–AktPH expressing cells were stimulated with PDGF for 5 min, at which time 250 μM LY294002 was added to rapidly inhibit further 3′ PI generation. The mean decay constant of the fluorescence intensity was determined to be 1.0 ± 0.4 min^{-1} (Fig. 6 D), in agreement with the model estimate. Also estimated was the parameter σ, the fold-increase in fluorescence intensity when a probe molecule is membrane-bound versus freely diffusing in the cytosol. Both the model and the experimental data in Fig. 1 C determined this quantity to be over an order of magnitude.

Though the analysis of the translocation kinetics at 37°C was confounded by changes in the shape of the contact area, the data was consistent with a moderately faster turnover rate ($\sim$1.5 min^{-1}) than at room temperature (Figs. 3 and 4, and data not shown). With this estimated turnover rate, the steady-state fluorescence profiles were consistent with a lipid diffusion coefficient not significantly affected by temperature in this range.

We also simulated the alternative situation where consumption of the second messenger is fast relative to diffusion, with the second messenger concentration at the center of the contact area being compensated by a nonzero generation rate (Fig. 6 E). In this case, the transition from the periphery to the center is too steep, and the model fails to predict a decrease in fluorescence for early time points. Also giving poor agreement with experiment was the situation where the second messenger generation rates are equal in the two domains, but the turnover rate is higher in the contact area (not shown). Thus, the observed radial variation in PDGF-stimulated fluorescence can be explained simply by lipid diffusion into the contact area from the nonadherent part of the cell.

Discussion

Our study introduces an evanescent wave imaging approach to investigate plasma membrane gradients in signaling components, a technique that offers significantly higher resolution than confocal microscopy. Using evanescent wave excitation of expressed GFP–AktPH, we found that 3′ PIs are involved in establishing cell orientation for directed motility of fibroblasts towards a PDGF source. This suggests that 3′ PI lipids play a general role in directed motility not only for G protein- but also for tyrosine kinase-mediated signaling processes. Intriguingly, the high sensitivity of evanescent wave imaging showed that most fibroblasts possess basal gradients in 3′ PI lipids, correlating with the polarization of the cell. The effect of adhesion on basal cell polarity is suggestive of a role for integrins in establishing 3′ PI gradients (Keely et al., 1997). Indeed, coupling between PDGF-induced migration and matrix interactions during wound healing has been suggested in previous studies (Xu and Clark, 1996; Greiling and Clark, 1997).

Our study also uncovered radial 3′ PI patterns in the cell–surface contact zone. Since it is likely that such a gradient enables 3′ PIs to selectively elicit actin cytoskeletal dynamics at the periphery of the contact area, we propose that the shape and size of the cell–surface adhesion area is regulated by this new type of lipid second messenger gradient. 3′ PIs may then have two roles, to promote directional motility via polar gradients and to define the shape of adherent cells via radial gradients in the contact area. Such radial gradients could uniquely contribute to optimal migration of cells that rely intimately on adhesion, like fibroblasts. This conceptual model of fibroblast motility based on polar and radial gradients is depicted in Fig. 7.

What are the biophysical implications for a spatial sensing mechanism involving 3′ PIs? To mediate spatial sensing, a polarity signal must act in a localized manner, proximal to the receptor. Two physical considerations argue that the modification of a membrane-associated molecule, such as a phospholipid, is an efficient way to accomplish this. First, receptor-mediated translocation of a cytosolic enzyme can then greatly amplify the observed affinity for the substrate and therefore the reaction rate (Haugh and Lauffenburger, 1997); importantly, this amplification is concomitant with enzyme–receptor association. Indeed,

recruitment of PI 3-kinase to the membrane is sufficient to enhance its observed activity, and translocation synergizes with allosteric effects resulting from binding the SH2 domains of the regulatory subunit (Klippel et al., 1996). Second, to maintain localization, a cytosolic signal would have to be consumed far more rapidly (a process requiring energy), since cytosolic proteins and small molecules diffuse much faster than membrane lipids and proteins (Schlessinger et al., 1977; Yokoe and Meyer, 1996; Swaminathan et al., 1997). The tight spatial regulation of cytosolic calcium is suggestive of a polarity signal, but a general role for Ca^{2+} in chemotaxis has failed to emerge (Pettit and Fay, 1998). In fibroblasts, Ca^{2+} may act prominently through the protease calpain, for two distinct functions in cell movement: increasing initial spreading by remodeling actin, and later weakening adhesions preferentially in the cell rear (Potter et al., 1998; Glading et al., 2000). A change in the distribution of intracellular calcium in fibroblasts over time (Hahn et al., 1992) may reflect the coordination of such functions, while 3′ PIs and perhaps other membrane signals remain more robustly localized at the leading edge.

The quantitative analysis of the diffusion profiles suggests that 3′ PI diffusion in the membrane is relatively unhindered, with localization achieved through a balance of diffusion and degradation rates. Given a diffusion coefficient of ~0.5 $\mu m^2/s$ and a lifetime of ~40 s, the range of produced 3′ PI lipids is <10 μm, explaining how polar as well as radial lipid second messenger gradients can readily be generated. By using a membrane-localized polarity signal, the cell can maintain these gradients with a modest rate of degradation, yet the 3′ PI turnover rate is sufficient to erase previous gradients in response to a redirection of the ligand source. Further, for a typical cell with 10,000 or more receptors, the diffusive nature of the polarity signal ensures that the contributions of perhaps several hundred receptors are spatially and temporally averaged. Such an integration of information from many partially ligated receptors is an important feature that could prevent the false perception of gradients in a uniform chemoattractant field (Tranquillo et al., 1988). Together, these considerations suggest that 3′ PIs and other rapidly degraded lipid second messengers are uniquely suited to serve as polarity signals for different cell functions.

References

Axelrod, D. 1981. Cell-substrate contacts illuminated by total internal reflection fluorescence. *J. Cell Biol.* 89:141–145.

Burmeister, J.S., L.A. Olivier, W.M. Reichert, and G.A. Truskey. 1998. Application of total internal reflection fluorescence microscopy to study cell adhesion to biomaterials. *Biomaterials.* 19:307–325.

Claesson-Welsh, L. 1994. Platelet-derived growth factor receptor signals. *J. Biol. Chem.* 269:32023–32026.

Czech, M.P. 2000. PIP2 and PIP3: complex roles at the cell surface. *Cell.* 100:603–606.

Deuel, T.F., R.S. Kawahara, T.A. Mustoe, and G.F. Pierce. 1991. Growth factors and wound healing: platelet-derived growth factor as a model cytokine. *Annu. Rev. Med.* 42:567–584.

Firtel, R.A., and C.Y. Chung. 2000. The molecular genetics of chemotaxis: sensing and responding to chemoattractant gradients. *BioEssays.* 22:603–615.

Frech, M., M. Andjelkovic, E. Ingley, K.K. Reddy, J.R. Falck, and B.A. Hemmings. 1997. High affinity binding of inositol phosphates and phosphoinositides to the pleckstrin homology domain of RAC/protein kinase B and their influence on kinase activity. *J. Biol. Chem.* 272:8474–8481.

Glading, A., P. Chang, D.A. Lauffenburger, and A. Wells. 2000. Epidermal growth factor receptor activation of calpain is required for fibroblast motility and occurs via an ERK/MAP kinase signaling pathway. *J. Biol. Chem.* 275:2390–2398.

Gray, A., J. van der Kaay, and C.P. Downes. 1999. The pleckstrin homology domains of protein kinase B and GRP1 (general receptor for phosphoinositides-1) are sensitive and selective probes for the cellular detection of phosphatidylinositol 3,4-bisphosphate and/or phosphatidylinositol 3,4,5-trisphosphate in vivo. *Biochem. J.* 344:929–936.

Greiling, D., and R.A.F. Clark. 1997. Fibronectin provides a conduit for fibroblast transmigration from collagenous stroma into fibrin clot provisional matrix. *J. Cell Sci.* 110:861–870.

Hahn, K., R. DeBiasio, and D.L. Taylor. 1992. Patterns of elevated free calcium and calmodulin activation in living cells. *Nature.* 359:736–738.

Haugh, J.M., and D.A Lauffenburger. 1997. Physical modulation of intracellular signaling processes by locational regulation. *Biophys. J.* 72:2014–2031.

Heldin, C., and B. Westermark. 1999. Mechanism of action and in vivo role of platelet-derived growth factor. *Physiol. Rev.* 79:1283–1316.

Hirsch, E., V.L. Katanaev, C. Garlanda, O. Azzolino, L. Pirola, L. Silengo, S. Sozzani, A. Mantovani, F. Altruda, and M.P. Wymann. 2000. Central role for G protein-coupled phosphoinositide 3-kinase γ in inflammation. *Science.* 287:1049–1053.

Kavran, J.M., D.E. Klein, A. Lee, M. Falasca, S.J. Isakoff, E.Y. Skolnik, and M.A. Lemmon. 1998. Specificity and promiscuity in phosphoinositide binding by pleckstrin homology domains. *J. Biol. Chem.* 273:30497–30508.

Keely, P.J., J.K. Westwick, I.P. Whitehead, C.J. Der, and L.V. Parise. 1997. Cdc42 and Rac1 induce integrin-mediated cell motility and invasiveness through PI(3)K. *Nature.* 390:632–636.

Klinghoffer, R.A., B. Duckworth, M. Valius, L. Cantley, and A. Kazlauskas. 1996. Platelet-derived growth factor-dependent activation of phosphatidylinositol 3-kinase is regulated by receptor binding of SH2-domain-containing proteins which influence Ras activity. *Mol. Cell. Biol.* 16:5905–5914.

Klippel, A., C. Reinhard, W.M. Kavanaugh, G. Apell, M. Escobedo, and L.T. Williams. 1996. Membrane localization of phosphatidylinositol 3-kinase is sufficient to activate multiple signal-transducing kinase pathways. *Mol. Cell Biol.* 16:4117–4127.

Kontos, C.D., T.P. Stauffer, W. Yang, J.D. York, L. Huang, M.A. Blanar, T. Meyer, and K.G. Peters. 1998. Tyrosine 1101 of Tie2 is the major site of association of p85 and is required for activation of phosphatidylinositol 3-kinase and Akt. *Mol. Cell. Biol.* 18:4131–4140.

Kundra, V., J.A. Escobedo, A. Kazlauskas, H.K. Kim, S.G. Rhee, L.T. Williams, and B.R. Zetter. 1994. Regulation of chemotaxis by the platelet-derived growth factor receptor-β. *Nature.* 367:474–476.

Lemmon, M.A., K.M. Ferguson, and J. Schlessinger. 1996. PH domains: diverse sequences with a common fold recruit signaling molecules to the cell surface. *Cell.* 85:621–624.

Li, Z., H. Jiang, W. Xie, Z. Zhang, A.V. Smrcka, and D. Wu. 2000. Roles of PLC-β2 and -β3 and PI3Kγ in chemoattractant-mediated signal transduction. *Science.* 287:1046–1049.

Martin, P. 1997. Wound healing: aiming for perfect skin regeneration. *Science.* 276:75–81.

Meili, R., C. Ellsworth, S. Lee, T.B.K. Reddy, H. Ma, and R.A. Firtel. 1999. Chemoattractant-mediated transient activation and membrane localization of Akt/PKB is required for efficient chemotaxis to cAMP in *Dictyostelium. EMBO (Eur. Mol. Biol. Organ.) J.* 18:2092–2105.

Niv, H., O. Gutman, Y.I. Henis, and Y. Kloog. 1999. Membrane interactions of a constitutively active GFP-Ki-Ras 4B and their role in signaling. *J. Biol. Chem.* 274:1606–1613.

Oancea, E., and T. Meyer. 1998. Protein kinase C as a molecular machine for decoding calcium and diacylglycerol signals. *Cell.* 95:307–318.

Parent, C.A., and P.N. Devreotes. 1999. A cell's sense of direction. *Science.* 284:765–770.

Parent, C.A., B.J. Blacklock, W.M. Froehlich, D.B. Murphy, and P.N. Devreotes. 1998. G protein signaling events are activated at the leading edge of chemotactic cells. *Cell.* 95:81–91.

Pettit, E.J., and F.S. Fay. 1998. Cytosolic free calcium and the cytoskeleton in the control of leukocyte chemotaxis. *Physiol. Rev.* 78:949–967.

Pierce, G.F., T.A. Mustoe, J. Lingelbach, V.R. Masakowski, G.L. Griffin, R.M. Senior, and T.F. Deuel. 1989. Platelet-derived growth factor and transforming growth factor-β enhance tissue repair activities by unique mechanisms. *J. Cell Biol.* 109:429–440.

Potter, D.A., J.S. Tirnauer, R. Janssen, D.E. Croall, C.N. Hughes, K.A. Fiacco, J.W. Mier, M. Maki, and I.M. Herman. 1998. Calpain regulates actin remodeling during cell spreading. *J. Cell Biol.* 141:647–662.

Rodriguez-Viciana, P., P.H. Warne, B. Vanhaesbroeck, I. Gout, M.J. Fry, M.D. Waterfield, and J. Downward. 1994. Phosphatidylinositol 3-OH kinase as a direct target of Ras. *Nature.* 370:527–532.

Rodriguez-Viciana, P., P.H. Warne, B. Vanhaesbroeck, M.D. Waterfield, and J. Downward. 1996. Activation of phosphoinositide 3-kinase by interaction with Ras and by point mutation. *EMBO (Eur. Mol. Biol. Organ.) J.* 15:2442–2451.

Sasaki, T., J. Irie-Sasaki, R.G. Jones, A.J. Oliveira-dos-Santos, W.L. Stanford, B. Bolon, A. Wakeham, A. Itie, D. Bouchard, I. Kozieradzki, et al. 2000. Function of PI3Kγ in thymocyte development, T cell activation, and neutrophil migration. *Science.* 287:1040–1046.

Schlessinger, J., D. Axelrod, D.E. Koppel, W.W. Webb, and E.L. Elson. 1977. Lateral transport of a lipid probe and labeled proteins on a cell membrane. *Science.* 195:307–309.

Schmoranzer, J., M. Goulian, D. Axelrod, and S.M. Simon. 2000. Imaging constitutive exocytosis with total internal reflection fluorescence microscopy. *J. Cell Biol.* 149:23–31.

Seppa, H., G. Grotendorst, S. Seppa, E. Schiffmann, and G.R. Martin. 1982. Platelet-derived growth factor is chemotactic for fibroblasts. *J. Cell Biol.* 92:584–588.

Servant, G., O.D. Weiner, P. Herzmark, T. Balla, J.W. Sedat, and H.R. Bourne. 2000. Polarization of chemoattractant receptor signaling during neutrophil chemotaxis. *Science.* 287:1037–1040.

Stauffer, T.P., S. Ahn, and T. Meyer. 1998. Receptor-induced transient reduction in plasma membrane PtdIns(4,5)P$_2$ concentration monitored in living cells. *Curr. Biol.* 8:343–346.

Swaminathan, R., C.P. Hoang, and A.S. Verkman. 1997. Photobleaching recovery and anisotropy decay of green fluorescent protein GFP-S65T in solution and cells: cytoplasmic viscosity probed by green fluorescent protein translational and rotational diffusion. *Biophys. J.* 72:1900–1907.

Teruel, M.N., T.A. Blanpied, K. Shen, G.J. Augustine, and T. Meyer. 1999. A versatile microporation technique for the transfection of cultured CNS neurons. *J. Neurosci. Methods.* 93:37–48.

Thompson, N.L., and B.C. Lagerholm. 1997. Total internal reflection fluorescence: applications in cellular biophysics. *Curr. Opin. Biotechnol.* 8:58–64.

Toomre, D., J.A. Steyer, P. Keller, W. Almers, K. Simons. 2000. Fusion of constitutive membrane traffic with the cell surface observed by evanescent wave microscopy. *J. Cell Biol.* 149:33–40.

Tranquillo, R.T., D.A. Lauffenburger, and S.H. Zigmond. 1988. A stochastic model for leukocyte random motility and chemotaxis based on receptor binding fluctuations. *J. Cell Biol.* 106:303–309.

Vanhaesebroeck, B., and M.D. Waterfield. 1999. Signaling by distinct classes of phosphoinositide 3-kinases. *Exp. Cell Res.* 253:239–254.

Watton, S.J., and J. Downward. 1999. Akt/PKB localisation and 3′ phosphoinositide generation at sites of epithelial cell–matrix and cell–cell interaction. *Curr. Biol.* 9:433–436.

Wennström, S., P. Hawkins, F. Cooke, K. Hara, K. Yonezawa, M. Kasuga, T. Jackson, L. Claesson-Welsh, and L. Stephens. 1994. Activation of phosphoinositide 3-kinase is required for PDGF-stimulated membrane ruffling. *Curr. Biol.* 4:385–393.

Whitaker, M. 2000. Fluorescent tags of protein function in living cells. *BioEssays.* 22:180–187.

Xu, J.H., and R.A.F. Clark. 1996. Extracellular matrix alters PDGF regulation of fibroblast integrins. *J. Cell Biol.* 132:239–249.

Yokoe, H., and T. Meyer. 1996. Spatial dynamics of GFP-tagged proteins investigated by local fluorescence enhancement. *Nat. Biotech.* 14:1252–1256.

Zigmond, S.H. 1996. Signal transduction and actin filament organization. *Curr. Opin. Cell Biol.* 8:66–73.